The spin orbital dynamics properties of vacancy diamond films using enhanced Raman scattering spectroscopy

R. REN[a,*], YIJING REN[a], XUAN LI[a]
Dept. of Optics, Xi'an Jiao Tong University, Xian, 710054, China

We investigated the Raman scattering spectrums of difference residual stress and thickness of diamond/Si films. The spin-orbital dynamics is caused by disordered lattice coupling and electron-phonons in diamond/Si. The diamond films were prepared on a Si substrate by MPCVD with methyl-hydrogen gas mixture. The Raman scattering spectrum of diamond/Si(100) hetero-junction was found as a function of crystal size, orientation, and film thickness. A sharp peak at 1360cm^{-1} is of D graphite sp^2, while the broad peak 1550 cm^{-1} of a broad band mode G, which corresponds to disordered sp^2 hybridization. The transfer of diamond sp^2 content extracted from C=C peak and converted to the sp^3 spin related effect. The diamond/Si(100) density state shows spin-related couple of sp^3, p and d orbital hybridization.

(Received April 13, 2017; accepted November 28, 2017)

Keywords: Diamond films, Nitrogen vacancy, Spin-orbit dynamics, Raman shift

1. Introduction

Nitrogen vacancy diamond is one of the most promising materials for the fabrication of optoelectronic power devices [1]. Semiconducting diamond is a most popular semiconductor with a wide band gap (5.45 ev), electric mobility 4500(cm^2/V.s), hole mobility 3800(cm^2/V.s), electric breakdown field 10000(KV/cm) and thermal conductivity 22 (W/K.cm) [2, 3]. The diamond surface could be a better alternative to oxygen terminated diamond for shallow NV centre. N type Si is a semiconductor with a wide band gap (3.37 ev) and large exciton binding energy (60 Mev) which potentially possesses the characteristics of high efficiency, light emitting, lower power and laser diodes. The doped diamond/Si hetero-structure displays charge carriers at the hydrogen-terminated surface of diamond and competition coupling of spin, lattice, and charge order. Meanwhile, Raman scattering is known to be a powerful technique to study the diamond/Si dynamics caused by electron-phonons [4-6]. Diamond is an electrical insulator but can withstand very high electrical fields. The hetero-structure diamond/Si induced a metallic state with high mobility in diamond and spin-related anomalous electrons transport behavior can be obtained [15]. Wu H reported on the improvement of single crystal diamond (SCD) nanoelectromechanical system (NEMS) resonators through annealing in oxygen [12]. Awschalom proposed a controlled spin of two NV centers in a optical cavity and driven by two off-resonant lasers with long spin coherence times and efficient single-Qubit quantum control [13]. Although Raman spectra of other diamond have been reported, there is no information on the lattice diamond in hetero-structure films as well as to analyze more specific aspects of phonon-electron interaction and isotopic doped nitrogen vacancy of diamond effects [14].

In this letter, we reported the different lattice orientation and grain size of diamond hetero-structure to investigate spin-related dynamics of different doped surface of diamond. The crystal diamond/Si(100) was prepared to explore charge transport and carrier injection of diamond/Si(100). A spin orbital coupling dependence of diamond energy band was observed in this junction that the diamond semiconductor had wide band gap, better electric mobility, high efficiency, [8, 9] resistive switching, [10-13], tunnel junctions [14,15], high-performance quantum information and ultraviolet fast-response device properties [15].

2. Experiments

The measurements were carried out on the diamond films on Si(100) single silicon substrate by the MPCVD with assisted microwave. Microwave reaction gas CH_4 and H_2 are inspired to produce ionization plasma. The ionization degree of reaction gas increased in 10% high density plasma [27].

The diamond (100) heterostructure thin films were fabricated on Si(100) substrate with microwave frequency 2.45GHz. The diamond (100) thin film of 720nm (estimated by SpecEI-2000-VIS ellipsometer) was deposited on Si(100) at the condition of hydrogen pressures 0.07 MPa, methane CH_4 pressures 4.9 MPa and 800°C. The diamond (100) thin films morphology had been observed by JEOL SEM scanning electron

microscope operating at the voltage of 25kV. The diamond/Si(100) structure was characterized by X-ray diffraction pattern at 300K shown in Fig. 1. The crystal size and orientation of deposited films were measured by XRD (Bruker D8 Advance XRD, smallest angular step 0.0001^0, 40mA, 40KV). Raman spectrums of films were recorded using the olid laser λ=632 nm, the power of 8mW at room temperature with a back scattering and were collected by Raman spectrometer (HR800, HORZBA, Jobin Yvon) equipped with confocal microscope and a nitrogen cooled charge-coupled detector. The spectrometer resolution was set at $4cm^{-1}$. Data were taken with a step size of 0.2 cm^{-1} over the (50-3000) cm^{-1} range to determine exact peak position and the FWHM.

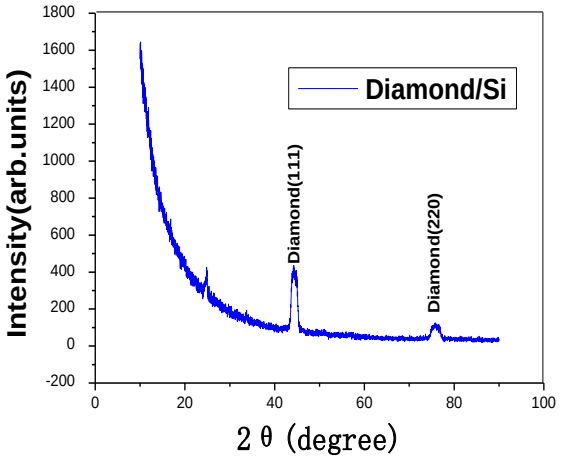

Fig. 1. The X-ray diffraction of diamond/Si(100) films. The diamond/Si(100) (111) and (220) diffraction peaks occurred at 2θ =44.258 ^{0}and 2θ =75.747^0

3. Results and discussion

Raman spectroscopy allows identifying different carbon allotropes in the sample. The Fig. 2 is shown Raman spectra of DLC fabricated by microwave assisted CVD. The sharp spectrum curve was fitted with Lorentzian diamond peak at 1332 cm^{-1} having FWHM of about 2 cm^{-1} and two Gaussian bands at 1360 cm^{-1} and 1550 cm^{-1}. In the same time, the Raman spectrum can be signed to the D-band of carbon and sp^2 -bonded carbon, respectively.

The films nucleation is the first step in diamond growth process. For CH_4-H_2, the dissociation gas brought large amounts of carbon and hydrogen atoms, which the group carbon is reconstructed on the surface of the substrates. It is easy to grow diamond homo-epitaxial junction on a single diamond crystal using MOCVD. Because of the atomic hydrogen etching on SP^2, the carbon atoms are far greater than SP^3 carbon atoms. After self-assembly of sample, SP^3 and C = C bond of the diamond structure are retained. The in-depth profile analysis shows that diamond layer closed to the interface of diamond has large compressive stress and the stress distribution along the film thickness is not distributed homogenously. The initial diamond nucleation process is very slow with nucleation density about $10cm^{-3}$. The micro-crystal have different shapes, did not show any preferential orientation in respect to the substrate at the beginning, and their size increase to the deposition time. The diamond Raman peak from the (111) crystal planes is almost twice broader in comparison to that from (100) crystal plane.

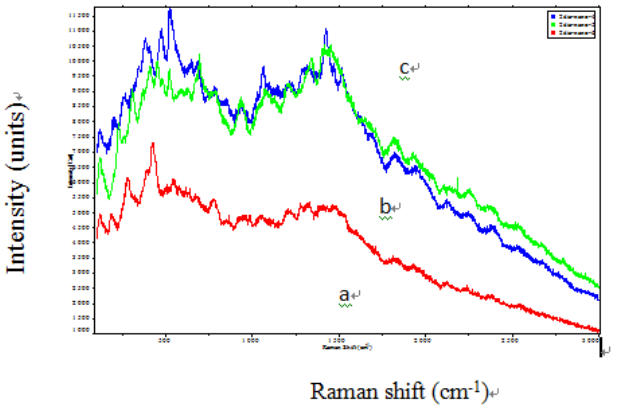

Fig. 2. The Raman spectra diamond/Si sample different crystal size scale of 5um(a),11um(b),13um (c)

The Raman spectrum indicated the diamond (111) crystal planes were more defective than (111) crystal planes shown in Fig. 2. The Raman spectrum taken from (111) crystal planes is twice broader than that from (100) crystal planes. The diamond/Si Raman spectrums of various crystal size and scales of 5um, 11um, 13um.(a,b,c) are indicated in Fig. 2. The FWHM on diamond crystal is dependence on crystal size, can be explained by the scale size effect but phonon confinement effect can not be ignored.

The diamond 2DHG has 2D holes gas 5 nm-10 nm below diamond surface. The diamond sp^2 extracts from π^* (C=C) peak and converts to the sp^3. It is so called spin coupling to the lattice strongly. Moreover, the C 1s-σ^* and C 1s-π^* coupling produce C=C bond due to the sp, sp^3, sp^2 strong correlation through anomalous magnetization respectively [10]. The reduced surface density is sensitive to metal potential function and has high carrier density 1×10^{13} (cm^{-2}).

Second, the nucleation density is increased about two orders of magnitude high than the previous case shown in Fig. 3. The growth of continuous polycrystalline diamond films begins with nucleation of individual crystallites on the surface defects. The crystal cells are growing increasingly, faceting and coalescence with neighboring crystallites, and finally growth of continuous layer in the perpendicular direction. The grain refinements showed diamond sample crystal belong to the cubic or faceted pyramid structures (space group: Fd$\bar{3}$m) with C=C band

and apical carbon sites. The XRD image indicated that the diamond/Si(100) (111) and (220) diffraction peaks occurred at 2θ =44.258 ^{0}and 2θ =75.747^0, diamond (100) FWHM 0.878, (200) FWHM 0.326, respectively, while the diamond diffraction peak occurred at 2θ =24.622^0, 25.306^0, 34.219^0, 43.555^0, 44.721^0, 75.075^0 shown in Fig. 1.

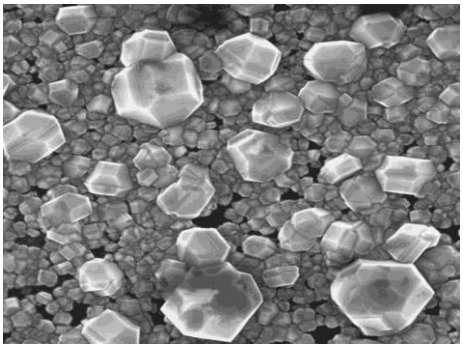

Fig. 3. The SEM microcopy of diamond/Si(100) films

Third, the surface SEM of diamond films exhibited predominantly faceted pyramidal structures and grains shown in Fig. 3, 4. The diamond morphology is imaged in Fig. 3. The laser confocal microscopy was used to detect in-depth profile analysis of diamond/Si(100) film in Fig. 4. As the laser close to the surface of diamond layer and the intensity increased, the Raman peak under strong compressive strain is shift +3.5 cm^{-1} due to diamond mono-crystal. The compressive stress reduces with increased distance from the wafer and is finally fully relaxed. When the distance is greater than 10um, the center position of Raman peaks is characteristics for diamond mono-crystal. Similar behavior indicates that the FWHM of diamond films is much sharp with increasing distance from the wafer. The Raman peak is broader while laser closes to the substrate.

Fourth, Raman spectrum peaks positions and their FWHM are changing in Fig. 5. Broadening of Raman peaks is caused by the increased strain stress or by reducing distance of diamond films. The diamond spectrum line becomes broader and low with decreasing crystal size. For diamond faceted pyramid in the Fd3 m space group, the factor group analysis yields two Raman-active phonon modes: 1332 and 1550 cm^{-1}. The Raman active phonon mode of diamond shows sharp first order Raman peak at 1332 cm^{-1}. High stress closed to the interface between the substrate and diamond between thermal origin because of difference between thermal expansion coefficients of diamond and substrate. The Raman spectrum also shows a broad band with maximum at 1550 cm^{-1}, which corresponds to the non-diamond and disordered graphitic carbon form with disordered sp^2 hybridization.

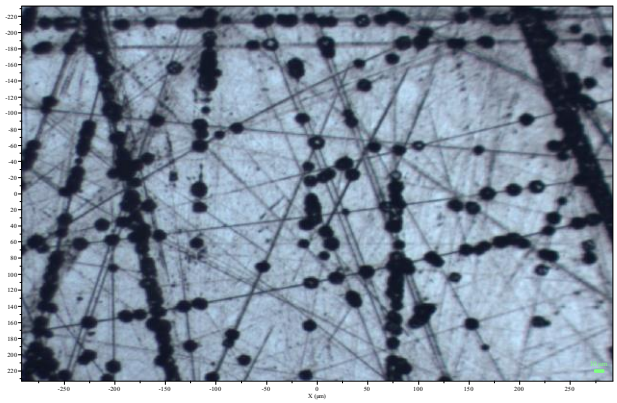

Fig. 4. The laser confocal microscopy of nanocrystal-diamond/Si(100) films

Fig. 5 shows the Raman spectra in-plane and inter-plane polarization respectively. The diamond spectrum line become broader and low with decreasing crystal size. The results are shown the line 1332cm^{-1} have been recognized as diamond crystals from sp^3 characteristic peak. A sharp peak at 1360 cm^{-1} indicates the formation of mode D, while the broad peak 1550 cm^{-1} of a broad band mode G, which corresponds to the nano-diamond with disordered sp^2 hybridization. The 1150 cm^{-1} corresponds to the nano-diamond. The transfer of diamond sp^2 content extracted from C=C peak and converted to the sp^3 spin related effect. A strong peak at 1332cm^{-1} indicates the formation of diamond, while the broad peak 1550 cm^{-1} of G indicates the formation of DLC. The 1132cm^{-1} and 1480 cm^{-1} are associated with hydrogen bonding of t-PA within film grain boundaries.

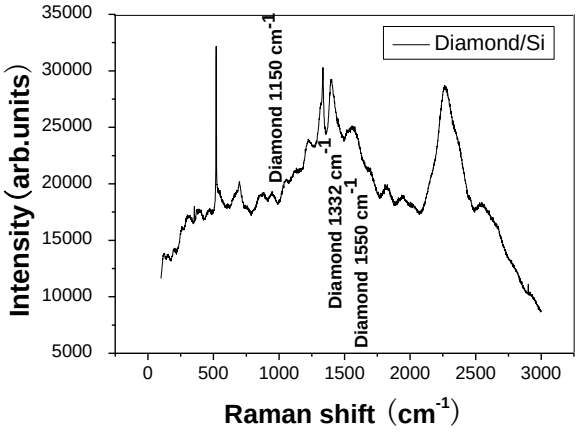

Fig. 5. The Raman spectra of diamond/Si(100) films of thickness 75nm. Raman scattering spectrum of diamond/Si(100) film with wavelength of 632 nm laser. The thickness is dependence on Raman scattering in polarization in diamond. The marked lines are a guide for the evolution of (C=C) phonon modes

For diamond/Si(100), Raman shift is shown in Fig. 5. The factor group analysis displays four Raman active phonon modes: 1150, 1332, 1360 and 1550 cm^{-1}. The group analysis yields three Raman active phonon modes. The bands near 1360 and 1550 cm^{-1} are generally known as D and G bands related with sp^2 islands. The D band appears due to the relaxation in the momentum selection rule of the Raman scattering SERS which belongs to small domain size shown in Fig. 5.

Fig. 6 shows energy band of the NV color center of diamond. NV color center can be thought as a three levels system. The ground state ^3A, metastable ^1A and excited state ^3E are a triplet states. The band gap between the ground state ^3A and excited state ^3E is 1.945 eV. Both of two states have zero field splitting corresponding to quantum number for $m_s=0$ and $m_s=\pm 1$. NV zero-field splitting in the ground state is about 2.88 GHz, which means that using a microwave can realize transition between $m_s=0$ and $m_s=\pm 1$ state. NV color centers have the special level structure whose nature is of great significance. We calculate the diamond NV energy band [19-21], as the result for direct band gap of 7.26 eV, the width of valence band of 25.84 eV. The diamond band gap calculated by the molecular orbital method is direct gap [22-26], which is the equivalent of energy difference of Brillouin zone Γ points.

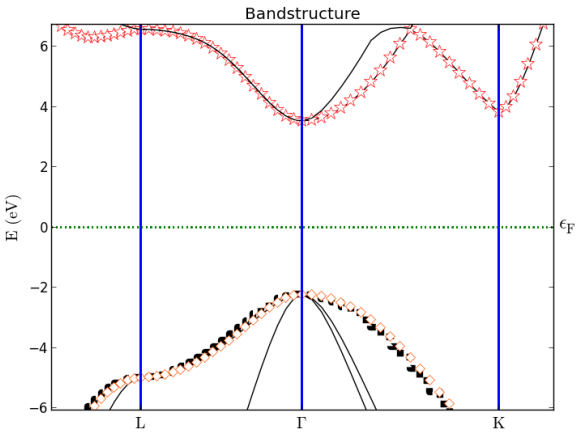

Fig. 6. The energy band of the diamond NV color center of Brillouin zone Γ points

4. Conclusions

In summary, the diamond films were fabricated successfully on N silicon substrate by using epitaxial MPCVD. We had present Raman scattering spectrum on the multilayer diamond/Si of spin related system. The spin transport dynamics made by the disordered spin-orbital coupling in diamond/Si. The results show that the diamond peak position and FWHM are dependence of the crystal size, orientation and strain stress. A strong peak at 1332cm^{-1} shows the formation of diamond. A peak at 1360cm^{-1} of D peak indicates the graphite sp^2, while the broad peak 1550 cm^{-1} of a broad band mode G, which corresponds to the nano-diamond and disordered graphitic carbon form with disordered sp^2 hybridization. We see that the size of diamond crystals increases linearly with deposition time. The FWHM depends on the crystal size. The diamond Raman peak from the (111) crystal planes is almost twice broader in comparison to that from (100) crystal plane. In-depth profile analysis shows that the diamond layers closing to the interface diamond are on compressive stress and the stress distribution along the thickness of films is not homogenous distributed. The energy band of diamond NV color center of Brillouin zone Γ points is 7.26 eV.

Acknowledgement

Supported by the National Natural Science Foundation of China under Grant Nos 61574115. Shaanxi Natural Science Basic Research Plan in Province of China (2016JM1029), XJTU Basic Research Plan (zdyf2017014) MOE Nonequilibrium Synthesis and Modulation and a Project Funded by the Priority Academic Program Development of JS Higher Education Institutions, PAPD, CICAEET.

References

[1] T. N. Makgato, E. Sideras-Haddad, M. A. Ramos, M. García-Hernández, A. Climent-Font, A. Zucchiatti, A. Muñoz-Martin, S. Shrivastava, R. Erasmus, Journal of Magnetism and Magnetic Materials **413**, 76 (2016).
[2] J. Michael Boteler, Y. M. Gupta, Phys. Rev. B **66**(1), 014107 (2002).
[3] A. I. Shames, V. Yu. Osipov, A. E. Aleksenskiy, E. Ōsawa, Diamond & Related Materials **20**(3), 318 (2011).
[4] K. Honda, T. Noda, M. Yoshimura, K. Nakagawa, A. Fujishima, J. Phys. Chem. B **108**(41), 16117 (2004).
[5] Ala'Eddin A. Saif, P. Poopalan, Optoelectron. Adv. Mat. **4**(12), 2008 (2010).
[6] S. Jin, T. H. Tiefel, M. McCormack, R. A. Fastnacht, R. Ramesh, L. H. Chen, Science **264**(5157), 413 (1994).
[7] Y. C. Wang, R. Ren, C. L. Chen, Canadian J. of Phys. **83**(7), 699 (2005).
[8] K. Hammerer, M. Wallquist, C. Genes, Phys. Rev. Lett. **103**(6), 063005 (2009).
[9] G Balasubramanian, P. Neumann, D. Twitchen, M. Markham, R. Kolesov, N. Mizuochi, J. Isoya, J. Achard, J. Beck, J. Tissler, Nature Materials **8**(5), 383 (2009).
[10] P. Rabl, Phys. Rev. Lett. **107**(6), 063601 (2011).
[11] P. W. May, C. A. Rego, C. G Trevor, E. C. Williamson, M. N. R. Ashfold, K. N. Rosser, N. M. Everitt, Diamond and Related Materials **3**(11-12),

1375 (1994).
[12] H. Wu, L. Sang, T. Teraji, T. Li, K. Wu, M. Imura, J. Q. You, Y. Koide, M. Y. Liao, Carbon **124**, 281 (2017).
[13] G Burkard, V. O. Shkolnikov, D. D. Awschalom, Phys. Rev. B **95**(20), 205420 (2017).
[14] A. Sawa, T. Fujii, M. Kawasaki, Y. Tokura, Appl. Phys. Lett. **85**(18), 4073 (2004).
[15] C. J. Tang, M. A. Neto, M. J. Soares, A. J. S. Fernandes, A. J. Neves, J. Grácio, Thin Solid Films **515**(7-8), 3539 (2007).
[16] J. R. Sun, Appl. Phys. Lett. **101**(15), 152901 (2012).
[17] Claire A. McLellan, Bryan A. Myers, Stephan Kraemer, Nano Lett. **16**(4), 2450 (2016).
[18] T. Shardaa, T. Soga, T. Jimbo, M. Umeno Diamond and Related Materials **9**(7), 1331 (2000).
[19] S. Jian, Z. Tianqi, H. Debiao, Z. Yuexin, S. Xingming, X. Yang, IEEE Trans. on Dependable and Secure Computing **7**(99), TDSC. 2725953 (2017).
[20] F. Zhangjie, W. Xinle, W. Qian, R. Kui, IEEE Trans. on Information Forensics and Security **12**(12), 2986 (2017).
[21] S. Jian, S. Jun, C. Xiaofeng, H. Xinyi, S. Willy, IEEE Trans. on Information Forensics and Security **12**(10), 2402 (2017).
[22] F. Zhangjie, H. Fengxiao, R. Kui, W. Jian, W. Cong, IEEE Trans. on Information Forensics and Security **12**(8), 1874 (2017).
[23] Z. Zhili, W. Yunlong, Y. Ching-Nung, S. Xingming, IEEE Trans. on Information Forensics and Security, **12**, 48 (2017).
[24] C. Yadang, H. Chuanyan, W. Wen, W. Enhua, Science China Information Sciences **59**(9), 1 (2016).
[25] T. Qing, C. Songcan, Neurocomputing **238**, 286 (2017).
[26] X. Zhihua, W. Xinhui, S. Xingming, W. Qian, IEEE Trans. on Parallel and Distributed Systems **27**(2), 340 (2015).
[27] M. Sobaszek, L. Skowronski, R. Bogdanowicz, Opt. Mater. **42**, 24 (2015).

*Corresponding author: ren@mail.xjtu.edu.cn